Astron. Astrophys. 333, 106–116 (1998)

ASTRONOMY AND ASTROPHYSICS

Starcounts in the flanking fields of the Hubble Deep Field⋆

The faint end of the disc stellar luminosity function and its scale-height

R.A. Méndez[1,⋆⋆] **and R. Guzmán**[2,3]

[1] European Southern Observatory, Karl-Schwarzschild-Strasse 2, D-85748 Garching b. München, Germany (rmendez@eso.org)
[2] Department of Astronomy, Yale University, P.O. Box 208101, New Haven, CT 06520-8101, USA (rguzman@astro.yale.edu)
[3] Hubble Fellow

Received 15 August 1997 / Accepted 10 November 1997

Abstract. We present instrumental (F606W, F814W) and calibrated (V, I) photometry and astrometry for point-like sources in the Hubble Deep Field and its flanking fields from combined HST and Keck direct imaging. From this data, a complete sample of stars in the range $18 \leq V \sim 25$ is derived and compared to the predictions of a galactic structure model. These comparisons allow to put constraints on the faint end of the disc's luminosity function (LF) as well as on the disc's scale-height. We find that a good representation for the faint disc's LF is provided by Stobie et al. (1989) for $M_v > +12$, with a slope $d\log\phi(M_v)/dM_v \sim -0.3$, quite different from the almost flat LF by Wielen et al. (1983) derived from the catalogue of nearby stars. This result confirms similar findings from other larger, but less homogeneous, HST samples. The observed red counts ($V - I \geq 3$) are best matched by a disc with a scale-height of 250 pc, rather than the "standard" value of 325 pc, in agreement with the determination of this parameter by Kroupa (1992) who uses a model that fully includes the effects of stellar binarity in the analysis of photometric parallaxes.

We explore the parameter space provided by the galactic model in order to find the best match to the observed starcounts and color counts. It is found that the best match advocates for a round "external" (Heliocentric distances of 8 to 10 kpc) halo, in agreement with recent findings from the kinematics of blue Horizontal-Branch stars (Wilhelm et al. 1996).

We find an equally good match between model and observations for a thick-disc with a local ("standard") normalization of 2% and a scale-height of 1300 pc (Reid & Majewski 1993), or a local normalization of 6% and a smaller scale height of 750 pc (Ojha et al. 1996). The ambiguity of the pair local-normalization to scale-height can not be resolved with star- and color-counts alone and other observational parameters are needed, as demonstrated by Robin et al. (1996) who favor the latter solution.

Key words: techniques: photometric – surveys – stars: distances – stars: late-type – Galaxy: fundamental parameters – Galaxy: structure

1. Introduction

The Hubble Deep Field (HDF, Williams et al. 1996) has provided outstanding insights into the evolution of Galaxies at high-redshift (for an updated list of publications derived from the HDF data see http://www.stsci.edu/ftp/science/hdf/hdf.html). Even though the number of faint stars in the field-of-view is quite small, they have also been used to test models of galactic structure, in particular with regards to the faint end of the luminosity function for the halo (Elson et al. 1996, Flynn et al. 1996, Méndez et al. 1996). Less well known and exploited have been the so-called Flanking Fields (FF), where HST performed observations of up to two orbits adjacent to the HDF to serve as alternative "pointings" for wide-field spectrographs.

In this paper we use the combined stellar sample derived from the HDF and FF, complemented with Keck imaging of the FF, to derive a larger stellar sample than that provided by the HDF alone. This sample which, of course, has a brighter limiting magnitude than that of the HDF, is then used to compare star- and color-counts with galactic model predictions to obtain constraints on the model parameters, mainly the disc's scale-height and luminosity function, the thick-disc scale-height, and the halo axial-ratio.

The paper is structured as follows: In Sect. 2 we present the HDF and FF data, with comparisons between the photometry derived for both sets of data. In Sect. 3 we present the details of the star- and color-counts modeling, including sample definition, completeness limits, and a detailed comparison to the observed counts for models with different parameters, along with a discussion of the best-match model parameters. Finally, in Sect. 4 we present our conclusions and recommendations for a possible HDF + FF survey toward other lines-of-sight in the Galaxy.

Send offprint requests to: R.A. Méndez

⋆ Based on observation obtained at the W. M. Keck Observatory, which is operated jointly by the University of California and the California Institute of Technology, and with the NASA/ESA Hubble Space Telescope, which is operated by AURA, Inc., under contract with NASA.

⋆⋆ *Present address:* Cerro Tololo Inter-American Observatory, Casilla 603, La Serena, Chile, (rmendez@noao.edu)

2. The data

2.1. Hubble Deep Field data

Méndez et al. (1996) have described the selection of point-like sources in the HDF, and have presented photometry for those objects. We have improved this previous photometry by incorporating simultaneous color constraints on the iterative procedure to convert from HST instrumental magnitudes to the Johnson-Cousin's system, and by applying full aperture corrections (generally small, see below). Our new calibrated photometry is presented in Table 1, which supersedes the calibrated photometry presented by Méndez et al. (1996). We use the same ID as that of Méndez et al. (1996), and we present now not only drizzled coordinates, but absolute coordinates as well.

In order to compare the point-like HDF photometry with that derived from the FF, it is necessary to have both photometries on the same instrumental system. Throughout this paper we have adopted the STMAG zero-points, while the magnitude system includes the energy encircled on a 0.5 arcsec radius of aperture on the WFPC2 (see Holtzman et al. 1995b, HB95 hereafter). The magnitudes presented by Méndez et al. (1996) were derived from SExtractor's "automatic-aperture magnitude" (AAM) routine (Bertin 1995, Bertin & Arnouts 1996), which are closely related to Kron's (1980) total magnitudes. Numerical simulations on SExtractor show that AAM measures approximately 94% of the total flux of the objects (Arnouts et al. 1996) and, consequently, there is a small offset between the total magnitudes and the AAM in the sense $m_{AAM} - m_{Tot} = +0.067$ mag, where m_{AAM} is the automatic-aperture magnitude derived from SExtractor and m_{Tot} is the total magnitude. Consequently we have applied this offset to our HDF data to compute m_{Tot}. In order to compute the corresponding magnitude encircled within an aperture of radius 0.5 arcsec, we have used the tables of encircled energy (EE) presented by Holtzman et al. (1995a, HA95 hereafter). These corrections have been computed for each passband separately, as the EE curves are dependent on the filter used. The final correction factors from m_{Tot} to $m_{0.5''}$ are the following:

$$m^{F450W}_{0.5''} = m^{F450W}_{Tot} + 0.118 \quad (1)$$

$$m^{F606W}_{0.5''} = m^{F606W}_{Tot} + 0.119 \quad (2)$$

$$m^{F814W}_{0.5''} = m^{F814W}_{Tot} + 0.098 \quad (3)$$

Table 1 indicates $m_{0.5''}$ derived from the above equations.

Calibrated photometry has been derived using the conversion equations given by HB95 in the way described by Méndez et al. (1996), but using an improved iterative procedure which fully exploits the color information available from the photometry. In both cases, however, we have explicitly considered the differences in zero-point between the STMAG system for HDF and those adopted by HB95 (including an offset due to the different detector gains used on the HDF (7 e^-/ADU) and that adopted by HB95 (14 e^-/ADU), which introduces a zero-point difference of 0.746 mag). Our improved photometry leads to fainter V magnitudes, redder $V-I$ colors and somewhat bluer colors in $B-V$ as compared to the HDF photometry by Flynn et al. (1996) and Elson et al. (1996). From Table 1 below and Table 2 in Méndez et al. (1996) we find that the mean differences (in the sense others - this work) are $\Delta V = -0.23 \pm 0.10$ and $\Delta(V-I) = -0.16 \pm 0.10$ with respect to the photometry by Flynn et al. (1996), while the mean differences for Elson et al. (1996) are $\Delta V = -0.53 \pm 0.14$, $\Delta(V-I) = -0.61 \pm 0.09$, and $\Delta(B-V) = +0.25 \pm 0.20$ (because of different selection criteria and apparent magnitude coverage, there are only nine objects in common between this three studies). The solid angle covered by the HDF data is 4.69 arcmin^2.

2.2. Flanking fields data

HST observed the FF only in the F814W filter. Integration times were one orbit for the "external" fields, and two orbits for the two fields just east and west from HDF. Detailed information on the distribution of flanking fields, integration times, etc., can be found on the STScI-HDF web pages (http://www.stsci.edu/ftp/science/hdf/project/flanking.html). In order to color-select targets for an spectroscopic follow-up of distant galaxies with Keck, the DEEP collaboration (http://www.ucolick.org/ deep/) has obtained a deep (300 sec exposure time) visual image of the FF with LRIS on Keck. The exposure was taken through a glass filter which combines a GG495 with a BG18 filter, and thus is not exactly similar to the Johnson's V filter. However, since the exposure was taken with the HDF in the center of the field, about 100 common objects between LRIS and HDF were used to define the transformation between LRIS visual magnitudes and F606W magnitudes, with an rms scatter of 0.15 mag.

A comparison with the objects detected on the HDF indicates that the 3σ magnitude limit of our Keck visual data is 27.4 in F606W (HST-STMAG system, within an aperture of radius 0.5 arcsec). Even though the solid angle covered by the HST-FF data (excluding the HDF) is 37.44 arcmin^2, we only have colors on a 24.62 arcmin^2 area, corresponding to the field-of-view of our LRIS image.

The point-like sample from the FF was derived solely based on the size of the images on the F814W frames. For this purpose, all objects with effective radius smaller than 0.16 arcsec were classified as point-like. Fig. 1 shows a plot of the logarithm of the effective radius as a function of an approximation to the Cousins-I magnitude from the F814W filter (for details on the derivation of source structural parameters, see Phillips et al. 1997). It is evident that our selection criteria is sufficient to separate point-like from extended objects at least down to 22.5 in I. Since the HDF data goes much deeper than this, we are, of course, dominated in our selection criteria by the shorter exposure times on the FF.

In order to derive magnitudes from Keck that are in the same system as those derived from the FF, the FF data were convolved with a PSF derived from the Keck data (this same PSF was used to derive photometry on the Keck image). Subsequently, magnitudes within an aperture of 1.12 arcsec (radius) were computed from both the Keck and the HST-degraded images (however the star-galaxy separation was performed on the full resolution

Table 1. Photometry & astrometry from HST for point-like sources on the Hubble Deep Field.

ID[a]	Chip[b]	X[c]	Y[c]	RA[d]	DEC[d]	F450W$_{0.5''}$	F606W$_{0.5''}$	F814W$_{0.5''}$	V	B-V	V-I
1	2	1920	1913	12:36:52.819	62:14:32.08	21.768	21.580	21.746	21.50	0.86	1.11
2	3	1221	507	12:36:53.664	62:13:08.27	22.846	22.240	22.101	22.29	1.24	1.54
3	4	742	600	12:36:46.762	62:12:37.08	25.207	24.189	23.283	24.39	1.57	2.43
4	3	1056	1056	12:36:54.045	62:12:45.60	25.773	24.568	23.592	24.77	1.81	2.50
5	3	2004	1188	12:36:59.301	62:12:55.82	25.858	24.795	23.389	25.05	1.56	2.94
6	4	380	597	12:36:45.974	62:12:50.40	25.967	25.280	25.177	25.31	1.37	1.49
7	4	410	1580	12:36:40.879	62:12:34.02	26.909	25.704	24.982	25.89	1.83	2.24
8	2	1950	840	12:36:47.145	62:14:15.96	25.256	25.996	26.380	25.83	-0.23	0.81
9	2	977	1272	12:36:51.638	62:13:47.43	27.498	26.582	26.265	26.70	1.55	1.78
10	2	906	1694	12:36:54.002	62:13:51.63	26.174	26.978	27.580	26.73	-0.21	0.50
11	2	627	583	12:36:48.846	62:13:23.61	27.688	28.218	28.523	28.09	0.00	0.92
12	3	1026	814	12:36:53.343	62:12:53.98	27.549	28.158	28.004	28.21	-0.34	1.56
13	4	1790	1306	12:36:45.381	62:11:47.66	28.064	28.510	28.793	28.39	0.10	0.95
14	2	625	249	12:36:47.105	62:13:18.17	27.928	28.853	28.669	28.92	-0.76	1.60
15	4	1193	1048	12:36:45.414	62:12:13.57	20.410	21.114	21.934	20.79	0.03	0.18
16	2	311	1573	12:36:54.735	62:13:28.00	21.193	20.486	20.359	20.53	1.38	1.52
17	3	1383	1321	12:36:56.357	62:12:41.13	19.655	——	20.106	——	——	——

[a] In Méndez et al. (1996) stars with ID= 15, 16, and 17 were not included because their analysis was concerned mainly with faint stars. Star 17 is saturated and unmeasurable in F606W. For the color and magnitude binning that will be performed here, the mild saturation on ID= 15 and 16 does not affect the counts (see Sect. 3.3).
[b] Chip refers to the WFPC2 chip in which the object appears.
[c] X and Y are the drizzled coordinates of the object (in pixels) on the respective Chip.
[d] Equinox is J2000.0

F814W images). This aperture was chosen as it corresponds to twice the FWHM (seeing disc) on the Keck data. Since this aperture contains more than 99% of the light, we have assumed in what follows that this aperture yields total magnitudes and, therefore, no aperture correction has been applied to bring this data into total magnitudes.

The total magnitudes derived in the fashion described above were then corrected to equivalent magnitudes on the HST-STMAG system within an aperture of radius 0.5 arcsec, in the same way as for the HDF data, i.e., using the EE tables presented by HA95, and Eqs. (2) and (3).

Table 2 shows the astrometry and photometry for our FF point-like sample, along with the derived Johnson-Cousin's calibrated photometry. Also, for a few objects, spectra have been taken, and their stellar nature confirmed, these are also noted in the Table.

2.3. HDF and FF data

Fig. 2 shows the combined HDF and FF color-magnitude diagram (CMD) in instrumental STMAG within an aperture radius of 0.5 arcsec. The agreement in the photometry between the two datasets is obvious, with the HDF data going, of course, much deeper. Fig. 2 also shows two stars (indicated by a star symbol, and not included on Table 2) identified spectroscopically by the DEEP collaboration. These objects, with radius slightly above 0.16 arcsec, were originally included in the "galaxy list", but turned out to be stellar objects. They fall in the middle of the color-magnitude distribution of stellar objects from the HDF+FF sample. In Fig. 2 we also indicate those objects from the point-like sample on the FF that have been spectroscopically confirmed as stars by various groups.

Elson et al. (1996) and Méndez et al. (1996) have argued, using the expected number-counts and the color-magnitude distribution of point-like objects respectively, that the point-sources derived from the HDF are likely to be essentially uncontaminated by QSOs. Because the objects detected on the FF cover a similar magnitude and color range as those found on the HDF (Fig. 2) we will assume in what follows that *all* of our HDF+FF sample, within the completeness limits specified below (see Sect. 3.1), consists of stellar objects.

3. Starcount modeling

In this section we present comparisons to the starcounts model by Méndez & van Altena (1996). The same model has been used to analize the faint starcounts from HDF alone by Méndez et al. (1996). Due to the increased area and sample provided by the FF it is now possible to address some issues that it was not feasible to address from the HDF data alone, namely, the adequacy of the present model to the intermediate-magnitude starcounts in the range $20 \leq V \leq 25$ and $V - I > 0$. We first define the sample, from the data presented in Sects. 2.1 and 2.2, and then we proceed to compare the counts on this sample to that predicted by the model.

Table 2. Photometry & astrometry from Keck and HST point-like sources on the Flanking Fields.

ID	Chip[a]	X[b]	Y[b]	RA[c]	DEC[c]	$F606W_{0.5''}$	$F814W_{0.5''}$	V	V-I	Spect. Conf.[d]
1	ie2	408	275	12:37:06.337	62:13:14.95	22.519	22.842	22.38	0.89	Cowie
2	ie3	1206	289	12:37:10.723	62:12:01.60	20.914	20.492	21.07	1.93	Cowie
3	ie2	546	365	12:37:05.944	62:12:58.74	23.755	22.711	23.96	2.57	Cowie
4	ie3	1362	625	12:37:07.241	62:11:33.95	24.598	24.434	24.65	1.57	
5	ie4	1213	1056	12:37:00.769	62:11:30.15	22.504	21.624	22.70	2.400	
6	ie4	968	1325	12:36:55.859	62:11:41.67	23.507	23.231	23.61	1.73	
7	iw2	231	221	12:36:37.569	62:14:54.73	26.152	23.437	26.74	4.41	
8	iw3	1308	352	12:36:42.046	62:13:11.29	25.735	24.308	25.99	2.96	
9	iw3	1503	584	12:36:40.133	62:12:44.22	22.995	21.919	23.21	2.60	
10	iw2	228	650	12:36:31.960	62:14:37.74	24.964	24.886	24.98	1.45	
11	iw2	696	653	12:36:34.607	62:13:54.97	24.233	24.116	24.27	1.51	
12	iw2	644	670	12:36:34.086	62:13:59.02	19.872	20.239	19.72	0.83	
13	iw2	279	728	12:36:31.235	62:14:30.00	26.488	24.876	26.77	3.16	
14	iw4	1454	954	12:36:35.026	62:12:33.86	24.482	24.165	24.60	1.78	
15	ne2	149	169	12:37:07.883	62:16:32.38	——	22.594	——	——	Cohen
16	ne2	345	215	12:37:08.412	62:16:12.68	——	21.345	——	——	
17	ne3	1312	453	12:37:10.852	62:14:34.95	22.719	23.110	22.55	0.80	
18	ne2	60	607	12:37:01.643	62:16:22.89	——	22.941	——	——	
19	ne3	1233	739	12:37:06.665	62:14:30.76	21.499	21.658	21.42	1.12	Cohen
20	ne3	940	773	12:37:04.539	62:14:55.98	21.275	21.723	21.09	0.72	Cohen
21	ne4	1389	794	12:37:06.840	62:14:14.33	24.391	23.609	24.58	2.30	
22	ne4	1257	1217	12:37:00.566	62:14:09.30	26.491	23.967	27.01	4.18	
23	ne4	1081	1369	12:36:57.566	62:14:19.24	23.210	22.715	23.39	2.02	
24	nw3	864	369	12:36:55.137	62:15:59.97	23.933	23.782	23.98	1.56	
25	nw3	1283	570	12:36:54.915	62:15:13.76	24.693	24.469	24.77	1.66	
26	nw3	1123	624	12:36:53.298	62:15:26.16	18.903	19.386	18.70	0.67	Cohen
27	nw4	1090	1333	12:36:43.857	62:15:00.64	23.020	21.782	23.25	2.77	
28	oe2	34	622	12:37:13.874	62:12:54.16	24.239	23.819	24.40	1.92	
29	oe2	180	644	12:37:14.415	62:12:39.96	21.809	22.116	21.68	0.92	Cowie
30	oe2	213	752	12:37:13.196	62:12:32.63	21.842	21.422	22.00	1.92	Cowie
31	oe4	1087	991	12:37:15.102	62:11:03.39	20.079	20.405	19.94	0.89	
32	ow3	1082	119	12:36:29.548	62:14:21.85	23.022	23.211	22.94	1.08	
33	ow2	456	264	12:36:24.064	62:15:13.04	——	23.978	——	——	
34	ow2	287	280	12:36:22.884	62:15:27.82	——	21.274	——	——	
35	ow3	1366	427	12:36:27.162	62:13:43.58	22.397	21.963	22.56	1.94	Cowie
36	ow4	944	1330	12:36:12.964	62:13:45.77	——	22.548	——	——	
37	se3	1161	130	12:36:56.677	62:10:03.27	——	22.872	——	——	
38	se2	316	134	12:36:51.789	62:11:20.14	27.204	24.587	27.76	4.29	
39	se2	147	134	12:36:50.820	62:11:35.52	23.193	22.392	23.38	2.32	
40	se3	1059	425	12:36:52.250	62:10:00.81	——	23.481	——	——	
41	se2	383	448	12:36:48.084	62:11:01.43	24.728	24.748	24.71	1.32	
42	se2	55	621	12:36:43.945	62:11:24.35	24.168	22.836	24.41	2.86	
43	se3	1509	631	12:36:52.150	62:09:11.49	——	——	——	——	
44	se3	1508	699	12:36:51.266	62:09:08.86	——	23.939	——	——	
45	se3	1107	728	12:36:48.579	62:09:44.24	——	20.042	——	——	
46	se4	973	1031	12:36:43.871	62:09:44.31	——	20.788	——	——	
47	se4	1490	1073	12:36:46.299	62:08:55.48	——	21.455	——	——	
48	se4	1160	1130	12:36:43.656	62:09:23.28	——	20.696	——	——	
49	se4	1008	1196	12:36:41.923	62:09:34.44	——	23.955	——	——	
50	se4	1028	1482	12:36:38.319	62:09:21.09	——	24.709	——	——	
51	sw4	844	1504	12:36:22.758	62:10:17.71	——	24.011	——	——	

[a] Chip refers to the two-letter code employed to identify the position with respect to the HDF, followed by the WFPC2 chip in which the object appears (visit the HDF web pages for a picture of the flanking fields with respect to HDF).
[b] X and Y are the coordinates of the object (in pixels) on the respective Chip.
[c] Equinox is J2000.0
[d] References are as follows: Cowie (unpublished); http://www.ifa.hawaii.edu/~cowie/hdf.html, Cohen (unpublished); http://astro.caltech.edu/~dwh/deep/hdf.html.

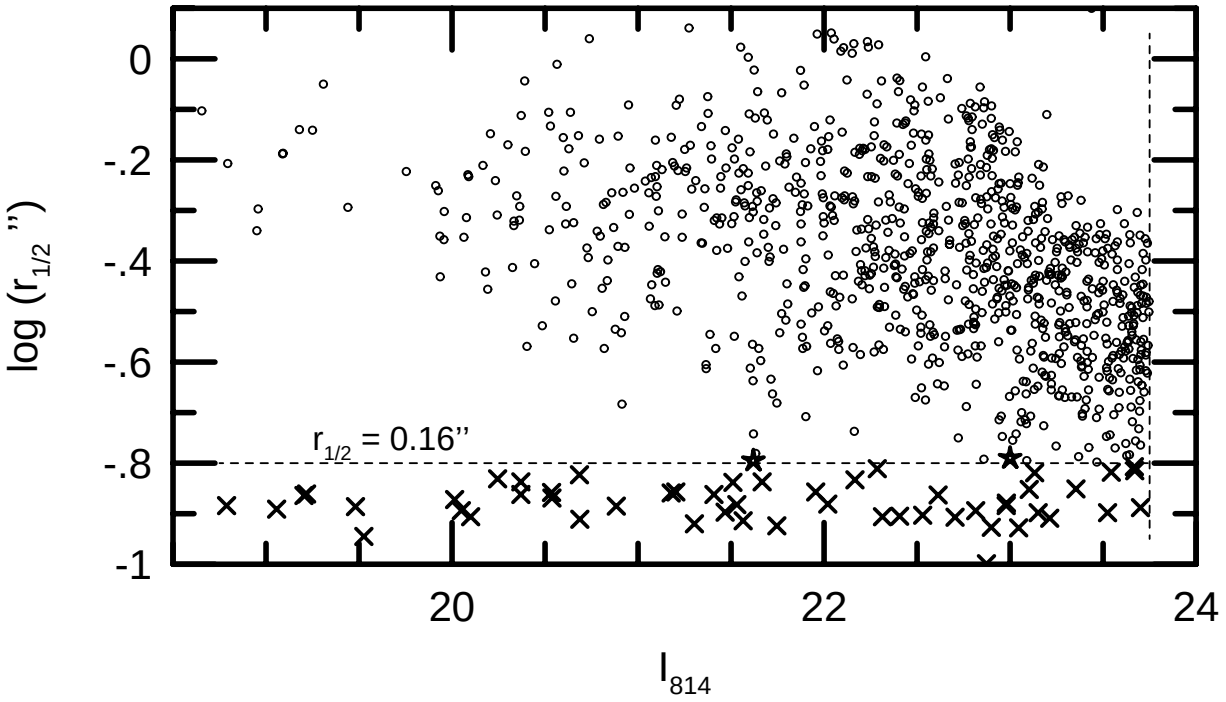

Fig. 1. Logarithm of the size of the images on the F814W frames *vs.* an approximation to the I-Cousin magnitudes for the whole FF data. The horizontal dashed line (at a half-light radius of 0.16 arcsec) indicates the boundary of our star-galaxy separation. The cut at I=23.74 has been artificially set as the magnitude limit for the determination of structural parameters of the detected sources, and for the spectroscopic follow-up of galaxies by the DEEP colaboration, and does not represents the actual limiting magnitude on the FF (Phillips et al. 1997). Point-like objects are shown as crosses, extended objects as open circles. Two objects with radius slightly above 0.16 arcsec, and which have been spectroscopically confirmed as stars, are shown by the star symbol.

3.1. Defining the sample

Because we have independent magnitude limits, V_{lim} and I_{lim}, the true magnitude limit, V^t_{lim}, is given as a function of color by $V^t_{lim} = Min\{V_{lim}; 0.5\times[(V-I)+V_{lim}+I_{lim}]\}$. The analyzed sample should therefore be restricted to the range $V \leq V^t_{lim}$. As said before, the Keck data has a (3σ) magnitude limit of $F606W_{0.5''} = 27.4$. This translates, using the HB96 magnitude transformations, to $V_{lim} \sim 27.7$ to 28.1 for objects in the color range $3.0 \leq V - I \leq 4.5$. On the other hand, the magnitude limit of the F814W data for the FF has been estimated using the exposure-time calculator (ETC) for WFPC2 available on the web pages of the Space Telescope European Coordinating Facility at http://ecf.hq.eso.org/. Since only two of the fields were observed for two orbits (total exposure time of 5300 sec), while all the others were observed for one orbit (total exposure time of 2500 sec), we used the exposure time of the shortest exposures to obtain a conservative estimate. We adopted the latest spectral type available on the calculator (a G5V spectra) as a representative of the spectra of the stars in the field, and specified a detector gain of 7 e^-/DN, as it was the case for *both* the HDF and the FF data. Using the ETC under this circumstances, the expected point-source S/N was recorded as a function of I magnitude. In this way, we find that an object with an I magnitude of 27 would have a S/N of 3.0 to 3.6 depending on whether it falls in the corner or in the middle of a WFPC2 pixel. We adopted, therefore, as a conservative value a 3σ limit of $I_{lim} = 27$ which corresponds to $F814W_{0.5''} = 28.0$.

As it can be seen from Fig. 1, the reliability of the star-galaxy separation fails at magnitudes fainter than $I = 23$, and therefore the relevant magnitude limit is not that imposed by the S/N of the sources ($I_{lim} = 27$) but, rather, by the classification. An optimistic look at Fig. 1 indicates that we can separate stars from extended objects down to $I = 23.0$, while a more conservative value would be 22.5 (corresponding to $F814W_{0.5''} = 24.3$ and 23.8 respectively). In what follows we adopt these limits to define our sample. Since these magnitudes are almost four magnitudes brighter than the expected 3σ magnitude limit on the WFPC2 data as computed from the ETC, we can say that our sample will be definetly complete at these magnitudes.

In Fig. 2 we indicate the magnitude limits at different levels which result from these constraints, where the horizontal line is defined by the magnitude limit on F606W, while the slanted lines indicate the restriction imposed by a magnitude limit in $F814W_{0.5''} \sim 23.8$ (pessimistic star-galaxy separation) or $F814W_{0.5''} \sim 24.3$ (optimistic star-galaxy separation). It is clear that it does not make too much difference for our statistical purposes on whether we adopt a pessimistic or an optimistic view on the magnitude limit for a reliable star-galaxy separation. As for the adopted magnitude limit in F606W to compare with the model counts, Fig. 2 indicates that we could assume a value closer to 20σ (i.e., $F606W_{0.5''} \sim 25.4$), or about 2 magnitudes

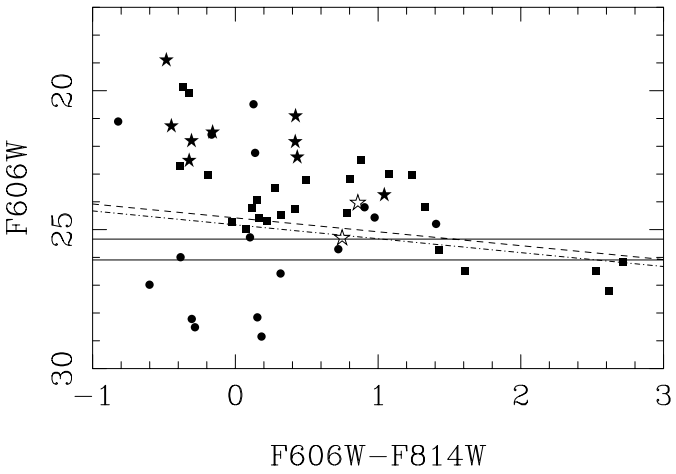

Fig. 2. Instrumental (STMag) color-magnitude diagram for our combined HDF + FF data. Filled circles are point-like objects from HDF, filled squares are point-like objects from the FF, filled stars are spectroscopically confirmed stars on FF, and open stars are the two spectroscopically confirmed stars with radius slightly above 0.16 arcsec (see Fig. 1). Solid lines are the 10σ (lower line) and 20σ (upper line) magnitude limits on $F606W_{0.5''}$, dashed line indicates the pessimistic star-galaxy separation boundary, with a 20σ magnitude limit on $F606W_{0.5''}$, while the dot-dashed line indicates the optimistic star-galaxy separation boundary with the same magnitude limit on F606W.

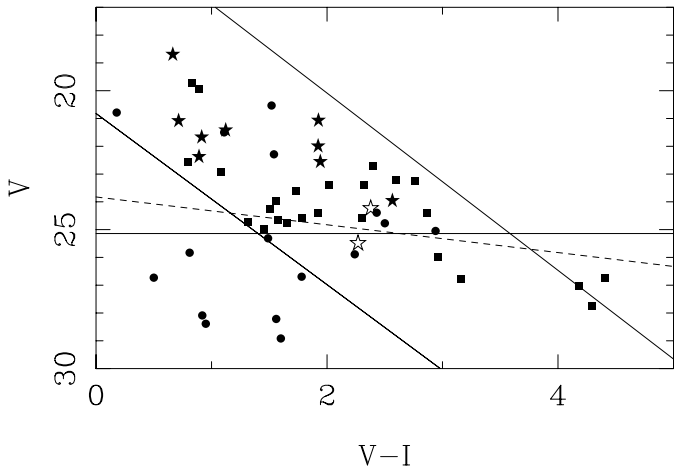

Fig. 3. Calibrated color-magnitude diagram for our combined HDF + FF data. Data symbols are as in Fig. 2. Horizontal line is the adopted magnitude limit on V (=25.15), dashed line is the corresponding magnitude limit in V for a magnitude limit on I of 22.5 (pessimistic star-galaxy separation) and on V of 25.15. Slanted solid lines indicate the locus of disc dwarfs at 1 kpc (upper, redder line) and of halo subdwarfs at 8 kpc (lower, bluer line).

brighter than the 3σ limit, thus ensuring, again, completeness of the data.

In Fig. 3 we show the calibrated CMD, with the corresponding magnitude limits. Our sample thus consists of 32 stars satisfying the constrain that they are brighter than the pessimistic star-galaxy separation line for $V - I < 2.65$ (i.e., $I < 22.5$), and brighter than 25.15 in V for redder colors (for consistency, the two spectroscopically confirmed stars with radius above 0.16 arcsec (see Fig. 1) have *not* been included in our statistical analysis, but their inclusion will not change our conlusions). The final magnitude limit in V has been imposed by taking the faintest star from HDF with $V - I = 2.94$, and adding an expected uncertainty of 0.1 mag in its photometry (see Table 1, ID=4). This magnitude limit is still about 0.5 mag *above* the 20σ limit on V and it is, therefore, an ultra-conservative trimming of the sample. In Fig. 3 we also show the locus for the lower (fainter) portion of the main-sequence (MS) for disc stars and for Subdwarfs, taken from the parallax study of Monet et al. (1992). For disc stars we have assumed a mean distance of 1 kpc, while for halo stars we have used a mean distance of 8 kpc. These assumed distances correspond to the typical distances for these objects in our sample, as predicted from the self-consistent distance distribution from the starcounts model (see Sect. 3.3). Since reddening is assumed to be zero, a change in distance only affects the ordinate but not the abcissa of the mean locus of disc and halo stars on Fig. 3.

3.2. Defining the model

The main characteristics of our starcounts model have been described by Méndez & van Altena (1996), Méndez et al. (1996), and Méndez & van Altena (1997). There are, however, two important issues in the context of this analysis that need to be addressed here. Firstly, the model was designed to predict starcounts in the Johnson's B and V passbands, where a suitable set of color-magnitude diagrams exist for the three populations included in the model (namely a disc, a thick-disc, and a halo). In order to perform predictions in V-I, it is necessary to provide the model with a transformation between B-V and V-I for the spectral types involved in this analysis. As it is clear from Fig. 3, we are looking at a dwarf population of stars. Indeed, the model predicts no giants or subgiants in this magnitude range (irrespective of color) in this field-of-view, and for any of the three galactic stellar populations included in the model. Therefore, only the calibration proper for MS stars needs to be addressed.

We have derived mean relationships for $B - V$ vs. $V - I$ from Reid & Gilmore (1982), and from Leggett (1992). The first paper gives a relation valid for MS stars in the color range $0.0 \leq B - V \leq 1.0$ and $0.0 \leq V - I \leq 1.0$, while Leggett (1992) gives a mean relationship for $1.1 \leq B - V \leq 2.2$ and $1.4 \leq V - I \leq 4.7$. Both relationships can be approximated with simple linear-piecewise fits, and in the range $1.0 \leq V - I \leq 1.4$ a linear interpolation between these two results has also been adopted. As emphasized by both Reid & Gilmore (1982) and Leggett (1992,) these color relationships hold independently of metallicity within the uncertainties of their photometry. Therefore, we have adopted these mean values for all three galactic components in the model. We have furthermore checked that variations in the slopes of these relationships,

within the observational uncertainties of the photometry from the studies by Reid & Gilmore and Leggett, do not affect in any way the conclusions presented below.

The luminosity function (LF) for the disc implemented by Méndez & van Altena (1996) includes Wielen's et al. (1983) LF for $M_v > +4$. For $M_v < -1$ Wielen's et al. function becomes increasingly incomplete (with only one star at $M_v = -1$, and 4 stars at $M_v = 0$ within 20 pc of the Sun), and we adopt instead McCuskey's function (1966) as a better representation in this absolute magnitude range. There is very good agreement in the region of overlap, $-1 \leq M_v < +4$, where we adopt the average of both functions (see Méndez & van Altena 1996). However, as we shall see, the HDF+FF data imposes some constraints on the faint end of the disc LF that indicate that the disc's LF is decaying rapidly for $M_v > +12$, as opposed to Wielen's et al. function which stays flat down to $M_v \sim +17$ and then decays abruptly. This result is not new, but since our data comprises a very small solid angle, with well defined observational constraints, this finding confirms in a satisfactory way similar results found from shallower starcounts, which include many lines-of-sight (i.e., a larger *effective* solid angle) having however varying amounts of reddening and different projection effects in the Galaxy which make the analysis more difficult (see, e.g., Santiago et al. 1996).

3.3. Starcounts model predictions

Even though we have increased the solid angle with respect to the HDF data by more than a factor of six by incorporating the FF data, the number of objets per unit of color or magnitude is still small, as it is evident from Fig. 3. Therefore, we have binned the data (and the model predictions) in coarse bins of magnitude and color. Furthermore, since there is a clear trend of decreasing apparent magnitude as the objects get redder, it is evident that fitting the observed starcounts to the model would be equivalent to fitting the observed color-counts, i.e., these two observables are not completely independent. For this reason, we have decided to concentrate on the color counts mainly, although we have checked that the magnitude counts are consistent as well (see Fig. 4).

Since general starcounts model have many free parameters that can be tuned-up to best match the observables, we present in what follows a number of simulations that indicate the expected change in the color-counts for a corresponding change of one of the model parameters, leaving all the other parameters untouched. This allows us to consider only those parameters that have the largest impact on the observables, and to maintain the other parameters fixed to a default value, therefore reducing effectively the degrees of freedom in the model. Rather than trying a full multi-parameter fit to the data, the purpose of this paper is to explore the sensitivity of the expected starcounts to different model parameters and to evaluate the usefulness of this type of data for issues of galactic structure, therefore adopting a more illustrative approach.

All of the model runs have been performed assuming a pessimistic view of our star-galaxy separation on the FF and, therefore, only the model counts in the range $18 \leq V \leq Min\{25.15; 0.5 \times [(V-I) + 25.15 + 22.5]\}$ have been computed (Fig. 3 shows the magnitude limits adopted in the model computations). Also, the color bins have been chosen to be 1 magnitude in $V - I$. As we shall see (Figs. 4 and 5), this allows a reasonable separation of the three stellar populations of the Galaxy while maintaining a reasonable number of objects per color bin, thus providing a clear picture of the parameter dependencies in the model.

Table 3 shows the observed color-counts as well as all of our model predictions (scaled to the field-of-view of the HDF+FF data, 29.31 arcmin^2). For all our model predictions we have adopted zero-reddening in $E(B-V)$. Run 1 in Table 3 has been performed with all the standard parameters described by Méndez & van Altena (1996). Fig. 4 compares the observed and predicted magnitude and color counts from this standard run. We can see that, while the bluer colors (and brighter magnitudes) are dominated by halo stars, the reddest (and faintest) objects do belong to the disc population, while the intermediate colors tend to be dominated by stars from the thick-disc.

Runs 2 to 5 indicate that, effectively, our model predictions are not very dependent on the height of the Sun from the galactic plane, nor on the solar Galactocentric distance. This can be explained because our counts include objects located mostly at distances larger than about 1 kpc, and therefore small uncertainties in these two parameters will not have an important effect on the predicted counts. Likewise, rather big variations in the adopted radial scale-length for the disc and thick-disc (runs 6 to 9), and the half-light radius for the halo (runs 12 and 13) do not have a large influence on the predicted counts. This is because the HDF+FF being located at $l \sim 126^\circ$ and $b \sim +55^\circ$ imply that starcounts do not sample a large range of Galactocentric distances, therefore reducing the model predictions to the adopted value of scale-lengths and the Solar-Galactocentric distance.

The situation is somewhat different with the adopted axial-ratio for the halo, specially when considering the bluest color bin which, at these magnitudes, it is expected to be dominated by stars from this population. A change of this parameter from 1.0 (spherical halo) to 0.5 (oblate halo, runs 10 and 11 respectively) induce a change of more than 70% in the predicted number of blue ($V-I < 1$) halo stars, as indicated in Table 3. By comparing with the observed number, it is obvious that the HDF+FF data favors a rounder halo, but the small number of stars in the bluest bin places only mild constraints on this parameter. The mean distance of these halo stars is predicted to be 8 kpc to 11 kpc, and thus sample the very outskirts of the stellar halo. Our indication of a round "external" halo is a more general phenomenon on the halo whereby nearby halo stars tend to show a flatter halo (as evidenced by their local kinematics), while deep starcounts (which sample halo stars at large Heliocentric distances) exhibit a rounder halo (see Freeman 1987 for a review of this problem). Our results seem to support the recent claim from the kinematic of field Horizontal-Branch stars that the halo has indeed two-components: An inner halo which is flattened and in prograde rotation, and an outer halo that is more spherical and in counter-rotation (Wilhelm et al. 1996).

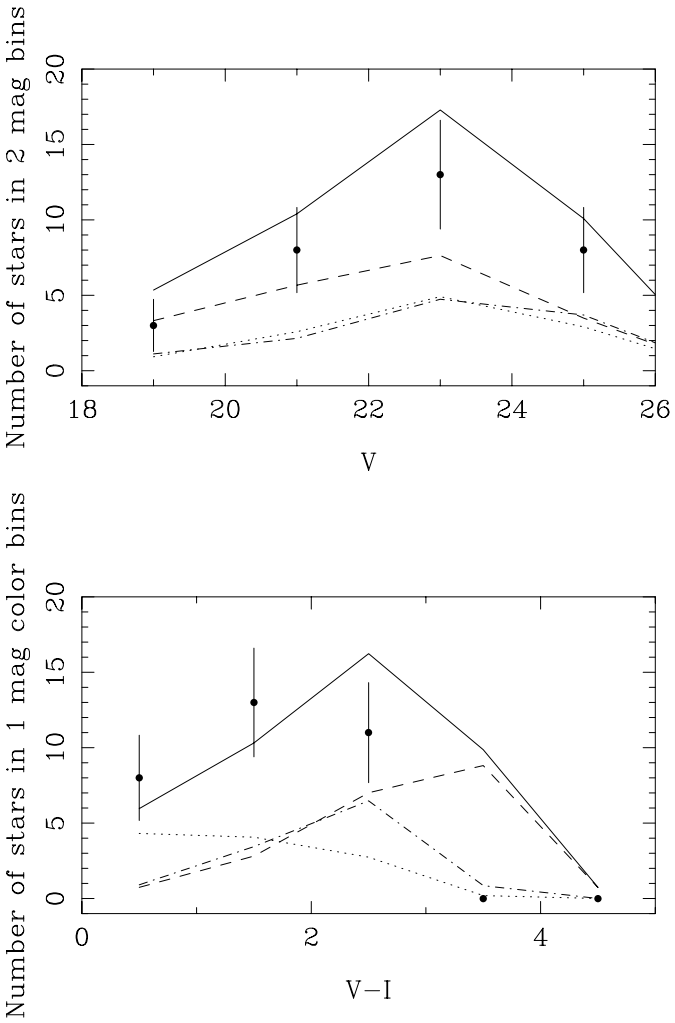

Fig. 4. Observed (solid dots with error bars) and predicted (lines) starcounts (upper panel) and color-counts (lower panel) from our run 1 (Table 3) using only standard parameters. Data symbols include only a 1σ Poisson uncertainty. The solid lines indicate the total counts predicted from the model, while the other lines show the disc (dashed), thick-disc (dot-dashed) and halo (dotted) contribution to the total predicted counts on both panels.

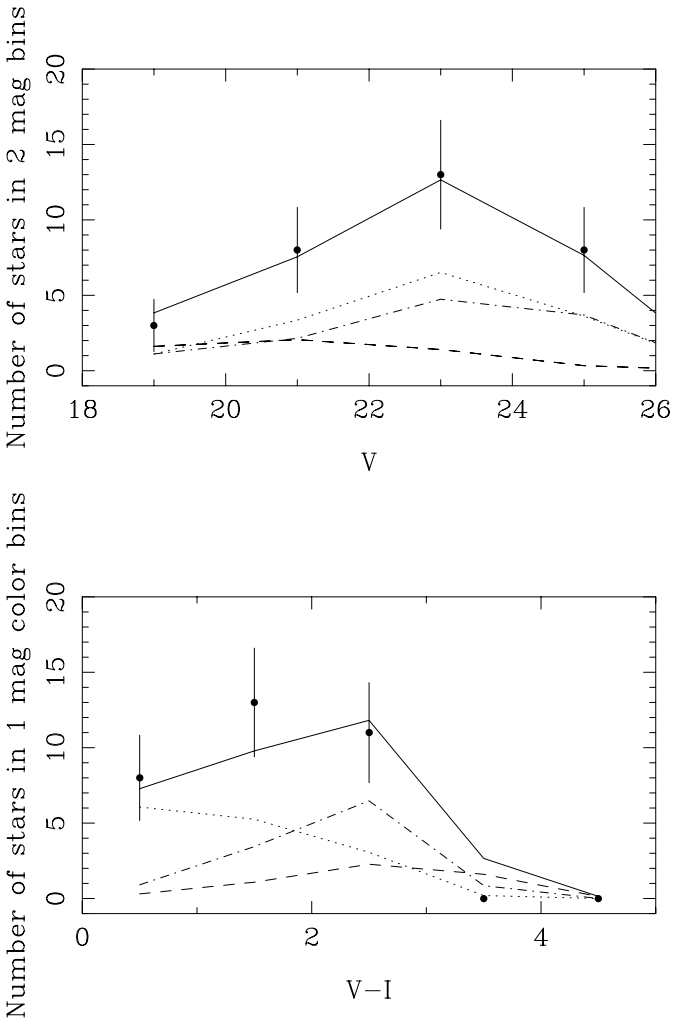

Fig. 5. Observed and predicted starcounts (upper panel) and color-counts (lower panel) from our best-fit model (run 31, Table 3), showing that a good fit to the color counts also produces a good fit the the starcounts. Same symbols as for Fig. 4.

Runs 14 to 17 indicate that the scale-height for disc and thick-disc stars have a large impact on the counts with the best solutions (runs 15 and 17) having a small scale-height for either the disc or the thick-disc. However, we see that the overall number of stars is best matched by run 15 having a disc with a scale-height of 250 pc and a thick-disc with a scale-height of 1300 pc. In all of the above computations we have used a local thick-disc normalization of 2%. Ojha et al. (1996) and Robin et al. (1996) have suggested a local normalization for the thick-disc of 5.6% with respect to the disc, larger than the classical value of 2% (see Reid & Majewski 1993 for a review of recent determinations). A change of normalization *does have* an impact on the preferred value for the thick-disc scale-height: Runs 19 to 22 show the predictions for an increased normalization for the thick-disc of 6%, and for various values of the scale-height of the thick-disc and disc. These predictions indicate a better fit in the color bin were the thick-disc dominates ($2 \leq V-I < 3$) for a scale-height of 750 pc, while for $V-I > 3$ a better fit is still obtained with a disc scale-height of 250 pc (run 22), as it was the case for the 2% normalization (because the thick-disc normalization does not affect the number of very red objects which are contributed mostly by the disc). The small scale-height found for the thick-disc with this higher local normalization is consistent with Robin's et al. claim of a scale-height of 760 ± 50 pc for this population, therefore indicating consistency in their argument that if we adopt a *larger* local normalization, then one must adopt as well a smaller scale-height. On the other hand, the small scale-height for the disc (which, as mentioned earlier, is mostly insensitive to the thick-disc normalization) agrees well with recent determinations of this parameter by Ojha et al. (1996) from multicolor counts and proper-motions on three fields in the direction of the galactic center, anti-center, and galactic rotation,

and with the determination by Kroupa (1992) who compares available determinations of this parameter with a model that fully includes the effects of stellar binarity.

It is interesting to notice that runs 1 to 22 indicate an overall overprediction for the number of stars in the reddest bins ($V-I>3$). These are expected to be mainly disc dwarfs at distances of about 1 kpc from the Sun. This discrepancy can be solved by adopting a LF for the disc with a decreasing number of stars for $M_v > +12$. As pointed out in Sect. 3.2, our standard model uses a Wielen's et al. (1983) LF, but recent HST results indicate that the faint end of the LF has fewer objects than those predicted by Wielen's et al. function. For example, Santiago et al. (1996) found from their analysis of 17 deep fields from the HST Medium Deep Survey, that the disc's LF has a slope of $d\log\phi(M_v)/dM_v \sim -0.178^{+0.056}_{-0.122}$ for $M_v > +13$, while Wielen's et al. function remains essentially flat down to $M_v \sim 17$ and then drops abruptly at fainter magnitudes. In order to test whether these results might have an impact on our overprediction on the number of red disc stars, run 23 shows the results of padding Wielen's et al. function for $M_v < +13$ with a decreasing LF for $M_v \geq +13$ having a slope of -0.178, similar to that found by Santiago et al. (1996), and with a scale-height for the thick-disc of 750 pc having a local normalization of 6% (i.e., as run 21). As it can be seen (compare runs 21 and 23), this does have an effect on the red counts, but not big enough to bring the model predictions into agreement with the observed counts. The following run (run 24), shows the predictions by adopting the lower slope of -0.3 found by Santiago et al., which does not predict a substantially different number of disc stars with respect to the previous run. However, as it can be seen from Fig. 5 in Santiago et al., Wielen's et al. function already has a higher stellar density at $M_v = +13$ than that found by Stobie et al. (1989). Consequently, run 25 presents the results from using Wielen's et al. function for $M_v < +12$, and Stobie's et al. (1989) LF at fainter magnitudes. In the range of overlap between these two determinations (i.e., $8 \leq M_v < +12$) there is very good agreement between these two determinations. Run 25 shows a much better agreement with our observed counts. Runs 23 to 25 used the "standard" disc scale-height of 325 pc, and a halo with an axial ratio of 0.8. Runs 26 and 27 show the predicted counts for a Wielen + Stobie LF with a small scale-height for the disc (250 pc) and a round halo (axial ratio of 1.0) respectively. As it can be seen from these two runs, the adoption of Stobie's et al. faint LF along with a smaller disc scale-height decreases even further the overprediction of red ($V-I \geq 3$) stars, while a rounder halo brings the bluer counts ($V-I<2$) in better agreement with the observed counts, the end result (run 27) being that the overall counts are better matched by this combination of parameters (32 observed stars *vs.* 30.5 stars predicted by the model).

Since runs 25 to 27, using Stobie's et al. LF, were performed with a 6% local normalization for the thick-disc, we may now go back to the 2% normalization to see what are the predictions with this new faint LF for the disc. Run 28 shows the predictions from the standard model (scale-height for the disc of 325 pc, scale-height for the thick-disc of 1300 pc and a local normalization of 2% for the latter), while runs 29 and 30 show the results of variations on the disc and thick-disc scale-heights adopting this lower thick-disc normalization. Run 31 shows the results for a model with a 2% thick-disc having a "standard" scale-height of 1300 pc and a round halo. From Table 3 we note that if we adopt a lower local normalization for the thick-disc, then we do not need to advocate a small scale-height for this component, although we still need a low scale-height for the disc. Indeed, we find that the number of stars predicted by the model in the intermediate colors $1 \leq V-I < 3$ for a thick-disc scale-height of 750 pc (run 30), is too small compared with the observed number, and that a better fit (runs 28, 29 and 31) is obtained by an *increased* thick-disc scale-height. However, an increase of the scale-height for the disc (run 28) leads to a larger than observed number of red stars, even for this decreasing luminosity function with a slope closer to $d\log\phi(M_v)/dM_v \sim -0.3$, as can be seen from run 28, thus ruling out this higher disc scale-height. We therefore conclude that the best solution in this case is obtained with a small scale-height for the disc, a large scale-height for the thick-disc, and a round halo. These results reinforce the "degeneracy" of the pair local normalization *vs.* scale-height for the thick-disc discussed before, but clearly point out to a small scale-height for the disc and to a round halo (see below).

Another point of interest is that all of the previous runs with a "standard" axial-ratio of 0.8 for the halo tend to underestimate the number of halo blue stars ($V-I<2$). This discrepancy can be resolved by increasing the axial ratio for the halo, as seen from runs 10 and 11. Run 27 shows the predictions for an axial ratio of 1.0 with the combined Wielen + Stobie LF for the disc in the case of a 6% thick-disc normalization, while run 31 shows the predictions in the case when a 2% normalization is adopted. We find that, irrespective of the adopted values for the disc and thick-disc, the best match to the blue counts is achieved by a round halo.

As a final note, we point out that the starcounts derived from the best-matching model to the color-counts do indeed agree with the observed magnitude counts. Fig. 5 shows the starcounts and color-counts from our run 31 as compared to the observed counts.

4. Conclusions

The basic conclusions of this paper can be summarized as follows:

- The red ($V-I \geq 3$) and faint ($18 < V \leq 25$) starcounts are best matched by a luminosity function similar to that of Wielen et al. (1983), except that at magnitudes fainter than $M_V > +12$ a better description is that provided by the LF by Stobie et al. (1989), with a slope of $d\log\phi(M_v)/dM_v \sim -0.3$, similar to the *smallest* slope from Santiago et al. (1996). A padding of Santiago's et al. LF to Wielen's et al. LF for $M_v > +13$ does not provide a satisfactory fit to the red starcounts.
- The scale-height for faint MS stars is closer to 250 pc than to the standard value of about 300-350 pc (Gilmore & Reid

Table 3. Predicted starcounts as a function of galactic structure parameters in the starcounts model.

Run	$0 \leq V-I < 1$	$1 \leq V-I < 2$	$2 \leq V-I < 3$	$3 \leq V-I < 4$	$4 \leq V-I < 5$	Total
Obs.	8	13	11	0	0	32
1	6.0	10.3	16.2	9.8	0.7	43.0
2	4.6	9.1	15.7	9.8	0.7	39.9
3	7.6	11.6	16.7	9.9	0.7	46.5
4	6.1	10.5	16.7	10.3	0.8	44.4
5	5.9	9.9	15.4	9.0	0.7	40.9
6	6.0	10.1	15.9	9.5	0.7	42.2
7	6.0	10.4	16.4	10.0	0.7	43.5
8	5.8	9.8	15.5	9.8	0.7	41.6
9	6.1	10.6	16.7	9.9	0.7	44.0
10	7.7	11.5	16.5	9.9	0.7	46.3
11	3.3	8.2	15.4	9.8	0.7	37.4
12	6.7	10.7	16.4	9.9	0.7	44.4
13	5.2	9.7	16.1	9.8	0.7	41.5
14	6.2	13.3	21.7	15.5	1.2	57.9
15	5.9	8.6	12.6	5.6	0.4	33.1
16	8.2	16.1	22.1	10.1	0.7	57.2
17	5.2	7.7	12.0	9.5	0.7	35.1
18	5.2	6.0	8.2	5.3	0.4	25.1
19	7.7	17.1	28.9	11.2	0.7	65.6
20	7.7	15.5	25.3	7.1	0.4	56.0
21	5.5	9.2	16.0	10.1	0.7	41.5
22	5.4	7.5	12.5	6.1	0.4	31.9
23	5.4	9.2	15.7	9.3	0.6	40.2
24	5.4	9.2	15.4	8.5	0.6	39.1
25	5.2	9.1	14.1	4.9	0.3	33.6
26	5.1	7.5	11.4	3.2	0.1	27.3
27	6.8	8.7	11.7	3.2	0.1	30.5
28	5.6	10.3	14.3	4.4	0.3	34.9
29	5.6	8.6	11.4	2.6	0.1	28.3
30	4.8	6.0	7.2	2.3	0.1	20.4
31	7.2	9.8	11.9	2.6	0.1	31.6

[a] The meaning of the different runs is discussed in the text. Here we give only a brief description.
Run 1: Standard parameters, as described in Méndez & van Altena (1996)
Run 2: $R_{\odot} = 7$ kpc; Run 3: $R_{\odot} = 10$ kpc
Run 4: $Z_{\odot} = -10$ pc; Run 5: $Z_{\odot} = +40$ pc
Run 6: Scale-length for disc stars of 2.5 kpc; Run 7: Scale-length for disc stars of 4.5 kpc
Run 8: Scale-length for thick-disc stars of 2.5 kpc; Run 9: Scale-length for thick-disc stars of 4.5 kpc
Run 10: Round halo (axial ratio= 1.0); Run 11: Oblate halo (axial ratio= 0.5)
Run 12: Half-light radius for the halo of 3.5 Kpc, Run 13: Half-light radius for the halo of 1.9 kpc
Run 14: Scale-height for disc MS of 400 pc; Run 15: Scale-height for disc MS of 250 pc
Run 16: Scale-height for thick-disc of 2 kpc; Run 17: Scale-height for thick-disc of 750 pc
Run 18: Scale-height for disc and thick-disc at 250 pc and 750 pc respectively
Run 19: Standard model, but local thick-disc normalization increased to 6%
Run 20: As run 19 but scale-height for disc decreased to 250 pc
Run 21: As run 19 but scale-height for thick-disc decreased to 750 pc
Run 22: As run 19 but scale-heights for disc and thick-disc decreased to 250 pc and 750 pc respectively
Run 23: As run 21 but mean disc LF from Santiago et al. (1996) for $M_v > +13$
Run 24: As run 23 but lower disc LF from Santiago et al. (1996)
Run 25: As run 21, but faint disc LF from Stobie et al. (1989) for $M_v > +12$
Run 26: As run 25 but a disc scale-height of 250 pc
Run 27: As run 26 but an axial ratio of 1.0 for the halo
Run 28: Standard parameters, but faint disc LF from Stobie et al. (1989)
Run 29: As run 28 but a disc scale-height of 250 pc
Run 30: As run 29 but a thick-disc scale-height of 750 pc
Run 31: As run 28 but an axial-ratio for the halo of 1.0

1983, van der Kruit 1986, Reid & Majewski 1993). This smaller value is in agreement with other determinations of this parameter when proper consideration of binarity is included in the analysis of the vertical distribution of the nearby stars (Kroupa 1992).

– From this data alone we can not decide between a larger local thick-disc normalization of 6% having a small scale-height of 750 pc, or a thick-disc normalized at 2% with a scale-height of 1300 pc. This ambiguity, clearly demonstrated in our simulations, has been found before by Reid & Majewski (1993). An analysis of other lines-of-sight, going to comparable magnitude limits, or the addition of kinematical information, could resolve this issue, as demonstrated by Robin et al. (1996) who analyzed star and color counts on a number of different intermediate-to-high galactic latitude fields from different surveys, and found a thick-disc with a scale-height of 760 ± 50 pc and a local normalization of 5.6 ± 1.0 %.
– The blue starcounts ($V-I \leq 1$) are best matched by a round "external" (Heliocentric distances of 8 to 10 kpc) halo, in agreement with recent findings from the kinematics of blue Horizontal-Branch stars (Wilhelm et al. 1996). This result is, however, tentative due to the small number of stars (only 8 observed stars) in this color bin.

A set of flanking-fields around the planned Southern Hubble Deep Field with photometry in, at least, V and I, will be most valuable to determine whether the results found from this Northern fields are also applicable toward other lines-of-sight in the Galaxy, with important bearings on the possible existence of long-lived structures (e.g., moving groups) in the disc and halo (Majewski et al. 1994, 1996).

An increased sample, such as that allowed by the addition of a Southern HDF + FF, will also help in putting stronger constraints on the parameters discussed here. An outstanding feature on Fig. 3 is the apparent slight excess of objects with $0.5 \leq V-I \leq 2.0$ and $23.5 \leq V \leq 25$ (see bottom panels on Figs. 4 and 5) which could still be interpreted as an *excess of thick-disc stars*. This excess has already been noticed by Santiago et al. (1996) from their analysis of the stellar sample derived from the HST Medium Deep Survey toward 17 high-to-intermediate galactic latitudes. However, due to the small sample size on HDF, even when including the FF, it seems advisable to wait until increased samples become available to study the significance of this excess which, as suggested be Santiago et al., might indeed reflect inadequacies in the galactic models proposed so far.

Acknowledgements. Dr. Richard Hook, from the Space Telescope European Coordinating Facility (ST-ECF), has provided much help in the determination of accuarte astrometry for the HDF point-sources presented here. The referee, Dr. Maria T. Ruiz, suggested several changes, particularly to Table 3, that have greatly improved the readability of the paper. We thank Jesús Gallego, James Lowenthal, and Drew Phillips for their help with the astrometry and data reduction, and David Koo for his help with the photometric calibrations. RG acknowledges partial support for this work from NASA grant AR-06337.08-94A and a Hubble Fellowship grant HF-01092.01-97A.

References

Arnouts S., de Lapparent V., Mathez G., et al. 1997, A&A submitted
Bertin E. 1995, SExtractor User's Guide, pub. Institute d'Astrophysique, Paris
Bertin E., Arnouts S. 1996, A&AS 117, 393
Elson R. A. W., Santiago B. X., Gilmore G. F. 1996, New Astronomy 1, 16
Flynn C., Gould A., Bahcall J. N. 1996, ApJ 466, L55
Freeman K.C. 1987, ARA&A 25, 603
Gilmore, G., Reid, N. 1983, MNRAS 202, 1025
Holtzman J., Hester J.J., Casertano S., et al. 1995a, PASP 107, 156 (HA95)
Holtzman J. A., Burrows C. J., Casertano S., et al. 1995b, PASP 107, 1065 (HB95)
Kroupa P. 1992, in Complementary Approaches to Double and Multiple Star Research, IAU Colloq. 135, ASP Conference Series, Vol. 32, H. A. McAlister and W. I. Hartkopf, 228
Leggett S.K. 1992, ApJS 82, 351
Majewski S. R., Munn J. A. Hawley, S. L. 1994, ApJ 427, L37
Majewski S. R., Hawley S. L., Munn J. A. 1996, in Formation of the Galactic Halo, Inside and Out, ASP Conference Series, Vol. 92, 1996, Heather Morrison and Ata Sarajedini, 119
McCuskey S. W. 1966, in Vistas in Astronomy, Vol. 7, A. Beer, Oxford: Pergamon, 141
Méndez R.A. 1995, Ph.D. Thesis, Yale University
Méndez R.A., van Altena W.F. 1996 A.J. 112, 655
Méndez R.A., Minniti D., De Marchi G., Baker, A., Couch, W. J. 1996, MNRAS 283, 666
Méndez R.A., van Altena W.F. 1997 A&A, in press
Monet D.G., Dahn C.C., Vrba F.J., et al. 1992, AJ 103, 638
Ojha D.K., Bienaymé O., Robin A.C., Crézé M., Mohan V. 1996, A&A 311, 456
Phillips A. C., Guzmán R., Gallego J., et al. 1997, ApJ, in press
Reid I.N, Majewski S.R. 1993, ApJ 409, 635
Reid N., Gilmore G. 1982, MNRAS 201, 73
Robin A.C., Haywood M, Crezé M, et al., 1996, A&A 305, 125
Santiago B.X., Gilmore G., Elson R.A.W. 1996, MNRAS 281, 871
Stobie R.S., Ishida K., Peacock J.A. 1989, MNRAS 238, 709
van der Kruit P.C. 1986, A&A 157, 230
Wielen R., Jahreiss H., Kruger R. 1983, in The nearby stars and the Stellar Luminosity Function, IAU Colloq. 76, A. G. Davis Philip and A. R. Upgren, Schenectady: L. Davis Press, 163
Wilhelm R., Beers T. C., Kriessler J. R., et al. 1996, in Formation of the Galactic Halo, Inside and Out, ASP Conference Series, Vol. 92, 1996, Heather Morrison and Ata Sarajedini, 171
Williams R. E., Blacker B., Dickinson M., et al. 1996 AJ 112, 1335